We are indebted to the College of Arts and Science of the University of Toledo for support of the X-ray facility and to F.-P. Ahlers for assistance with the crystallography.

Supplementary Material Available: Tables S1-S6, listing experimental details for the structure determination, thermal parameters, derived hydrogen positions and thermal parameters, and complete bond distances and angles (6 pages); Table S7, listing calculated and observed structure factors (5 pages). Ordering information is given on any current masthead page.

Contribution from the Chemistry Departments, University of Virginia, Charlottesville, Virginia 22901, and North Dakota State University, Fargo, North Dakota 58105

Matrix-Infrared Spectra of Structural Isomers of the Phosphorus Oxysulfide P_4S_3O

Zofia Mielke,[†,‡] Lester Andrews,*[,†] Kiet A. Nguyen,[§] and Mark S. Gordon*[,§]

Received February 5, 1990

Photolysis of the P_4S_3--O_3 molecular complex in solid argon with red light produced two sets of new infrared absorptions including terminal PO and symmetric P-S-P stretching modes, which are assigned to structural isomers of P_4S_3O with terminal oxygen at the apex and base phosphorus positions of P_4S_3. Further ultraviolet photolysis produced evidence for oxo-bridged P_4S_3O and a secondary product, $P_4S_3O_2$.

Introduction

The simplest stable phosphorus sulfide, tetraphosphorus trisulfide, P_4S_3, was discovered by Lemoine in 1864.[1] The bird-cage C_{3v} structure for P_4S_3 has been determined by electron and X-ray diffraction of the vapor and solid phases, respectively.[2,3] According to infrared and Raman spectra of the solid, molten phase, and vapor, P_4S_3 retains the same structure in all three phases.[4] Mass spectra of the vapor show that the molecular ion $P_4S_3^+$ is the most abundant species.[5,6]

Phosphorus oxysulfides are typically prepared by reacting P_4O_{10} or P_4O_6 with P_4S_{10}, which give a range of higher oxysulfides $P_4O_{10-n}S_n$ (n = 2-9).[7,8] However, the oxidation of P_4S_3 in solution with oxygen gas yields a lower oxide of formula $P_4S_3O_4$.[9,10] Matrix reactions with ozone have proven to be a fruitful method for oxidizing phosphorous; red light photolysis of the P_4--O_3 complex in solid argon has produced the terminally bonded P_4O isomer as characterized by infrared spectroscopy.[11,12] An analogous matrix-infrared study of P_4S_3 and O_3 is reported here. Of particular interest is the addition of terminal oxygen to the two different phosphorus positions in the P_4S_3 molecule and the formation of two terminal-oxygen P_4S_3O isomers. To aid in interpretation of the experimental results, electronic structure calculations on P_4S_3O isomers are presented as well.

Experimental Section

The closed-cycle refrigerator, Perkin-Elmer 983 spectrometer, high-pressure mercury arc lamp, vacuum apparatus, and techniques for preparing matrix samples containing ozone have been described previously.[11-13] Ozone was synthesized from normal isotopic, 50% and 98% ^{18}O-enriched oxygen gas. High-resolution infrared spectra were recorded; wavenumber accuracy is ±0.3 cm^{-1}. Tetraphosphorus trisulfide, P_4S_3, obtained from Fluka was evaporated from a quartz or stainless-steel Knudsen cell at 100-110 °C into argon or Ar/O_3 = 150/1 or 75/1 streams and condensed on a cesium iodide window maintained at 12 K. Infrared spectra were recorded, samples were photolyzed with a high-pressure mercury arc (1000 W) using 290-, 420-, and 590-nm glass cutoff and water filters, and more spectra were recorded. After the matrix samples were evaporated, a yellowish white powder, presumably $P_4S_3O_4$, remained on the window.

Electronic structure theory calculations were performed using the effective core potentials[14] recently added to GAMESS.[15] Molecular structures and vibrational frequencies were determined at the self-consistent field (SCF) level of theory, while the final relative energies were obtained with second-order perturbation theory (MP2),[16] at the SCF geometries. For all calculations, a set of six d orbitals was added to each atom, using the exponents from the 6-31G(d) basis sets.[17]

Table I. Infrared Absorptions Produced by Photolysis of P_4S_3--O_3 Samples in Solid Argon at 12 K

group 1		group 2		other	
^{16}O	^{18}O	^{16}O	^{18}O	^{16}O	^{18}O
1218.4	1176.3	1251.0 sh	1207.1 sh	1281.5	1237.5
558.8	557.2	1247.4	1203.9	1262	1219
251.4	248.6	538.3	537.8	753	723
212.3	209.2	500.2	500.0	727	698
		467.5	467.5	523	
		279.3	269.7		

Results

The infrared spectrum of P_4S_3 isolated in solid argon revealed two very strong absorptions at 446 and 429 cm^{-1}, two strong bands at 490 and 224 cm^{-1}, and two medium-intensity bands at 346 and 292 cm^{-1}. These bands are 2-6 cm^{-1} higher than peaks reported for P_4S_3 in a Nujol mull.[4] Photolysis of the matrix sample with 590-1000- and 220-1000-nm radiation for 1-h periods produced no changes in the infrared spectrum.

The codeposited sample containing P_4S_3 and O_3 revealed ozone bands[11] at 1104, 1040, and 704 cm^{-1}, the above P_4S_3 absorptions,

(1) Lemoine, G. *C. R. Hebd. Seances Acad. Sci.* **1864**, *58*, 890.
(2) Akishin, P. A.; Rambidi, N. G.; Ezhov, Yu. S. *Russ. J. Inorg. Chem. (Engl. Transl.)* **1960**, *5*, 358.
(3) Leung, Y. C.; Waser, J.; Van Houten, S.; Vos, A.; Wiegers, G. A.; Wiebenga, E. H. *Acta Crystallogr.* **1957**, *10*, 574.
(4) Gardner, M. *J. Chem. Soc., Dalton Trans.* **1973**, 691.
(5) Penny, G. J.; Sheldrick, G. M. *J. Chem. Soc. A* **1971**, 243.
(6) Muenow, D. W.; Margrave, J. L. *J. Inorg. Nucl. Chem.* **1972**, *34*, 89.
(7) Walker, M. L.; Peckenpaugh, D. E.; Mills, J. L. *Inorg. Chem.* **1979**, *18*, 2792.
(8) Wolf, G.-U.; Meisel, M. *Z. Anorg. Allg. Chem.* **1984**, *509*, 111.
(9) Stock, A.; Friederici, K. *Ber. Dtsch. Chem. Ges.* **1913**, *46*, 1380.
(10) Hoffman, H.; Becke-Goehring, M. Phosphorus Sulfides. In *Topics in Phosphorus Chemistry*; Griffith, E. J., Grayson, M., Eds.; John Wiley and Sons: New York, 1976; Vol. 8, pp 193-271.
(11) Andrews, L.; Withnall, R. *J. Am. Chem. Soc.* **1988**, *110*, 5605.
(12) Mielke, Z.; Andrews, L. *Inorg. Chem.* **1990**, *29*, 2773.
(13) Andrews, L.; Spiker, R. C. *J. Phys. Chem.* **1972**, *76*, 3208.
(14) Stevens, W. J.; Basch, H.; Krauss, M. *J. Chem. Phys.* **1984**, *81*, 6026.
(15) (a) Dupuis, M.; Spangler, D.; Wendoloski, J. J. NRCC Software Catalog Program QG01, 1981. (b) Schmidt, M. W.; Baldridge, K. K.; Boatz, J. A.; Koseki, S.; Gordon, M. S.; Elbert, S. T.; Lam, B. *QCPE* **1987**, *7*, 115.
(16) Pople, J. A.; Binkley, J. S.; Seeger, R. *Int. J. Quantum Chem.* **1976**, *S10*, 1-19.
(17) (a) Hariharan, P. C.; Pople, J. A. *Theor. Chim. Acta.* **1973**, *28*, 213. (b) Gordon, M. S. *Chem. Phys. Lett.* **1980**, *76*, 163. Krishnan, R.; Frisch, M. J.; Pople, J. A. *J. Chem. Phys.* **1980**, *72*, 4244.

[†] University of Virginia.
[‡] On leave from University of Wroclaw, Wroclaw, Poland.
[§] North Dakota State University.

0020-1669/90/1329-5096$02.50/0

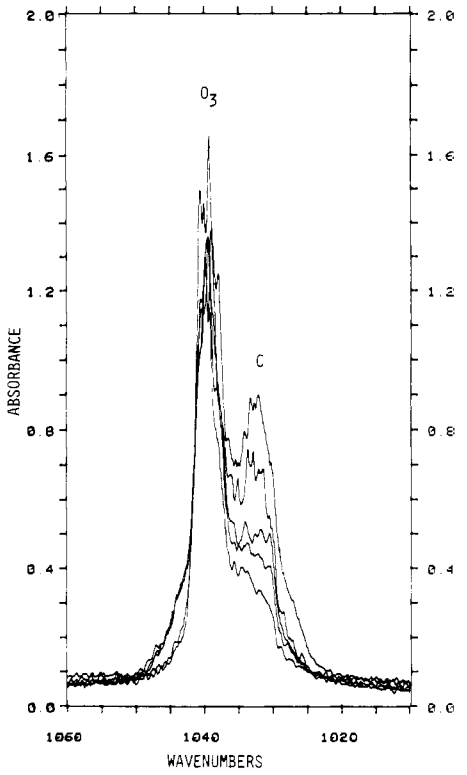

Figure 1. ν_3 band of O_3 in the spectra of P_4S_3 codeposited with Ar/O_3 = 150/1 immediately after deposition (top) and after subsequent 20, 60, and 110 min of 590-1000-nm photolysis and 30 min of 420–1000-nm photolysis. The C band decreases gradually with prolonged photolysis time.

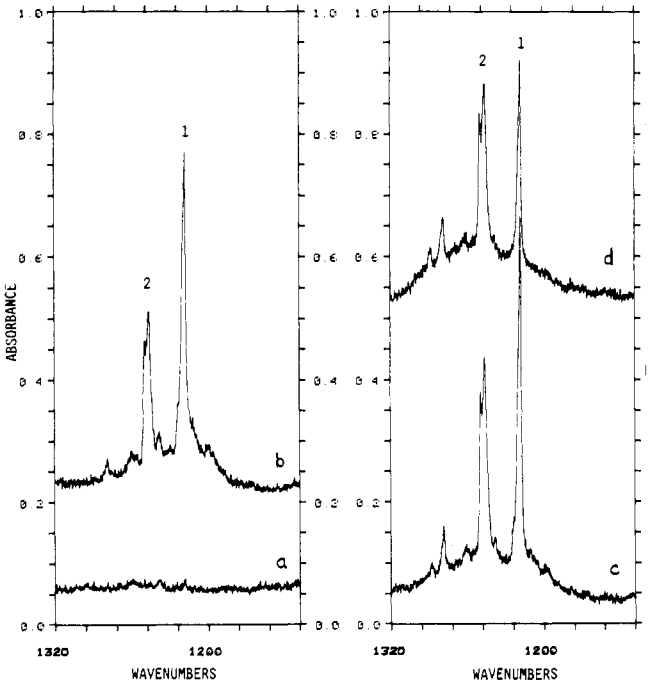

Figure 2. Terminal P–O stretching region in the spectra of P_4S_3 codeposited with Ar/O_3 = 75/1: (a) immediately after deposition; (b) after 90 min of 590–1000-nm photolysis; (c, d) after 30 (c) and 210 min (d) of 220–1000-nm photolysis.

and new ozone satellite bands at 1101.5, 1032.2, and 700.1 cm^{-1}. The strong 1032.2-cm^{-1} band (labeled C) and its photolysis behavior are shown in Figure 1. Photolysis with red light ($\lambda > 590$ nm) for 30 min markedly reduced the C bands, and produced two groups of new bands labeled 1 at 1281.4, 558.8, 251.4, and 212.3 cm^{-1} and labeled 2 at 1247.4, 538.3, 500.2, 467.5, and 279.3 cm^{-1} in Figures 2 and 3. Red photolysis for 30 min gave a substantial yield of bands 1 and 2; further red-light photolysis for 60 min

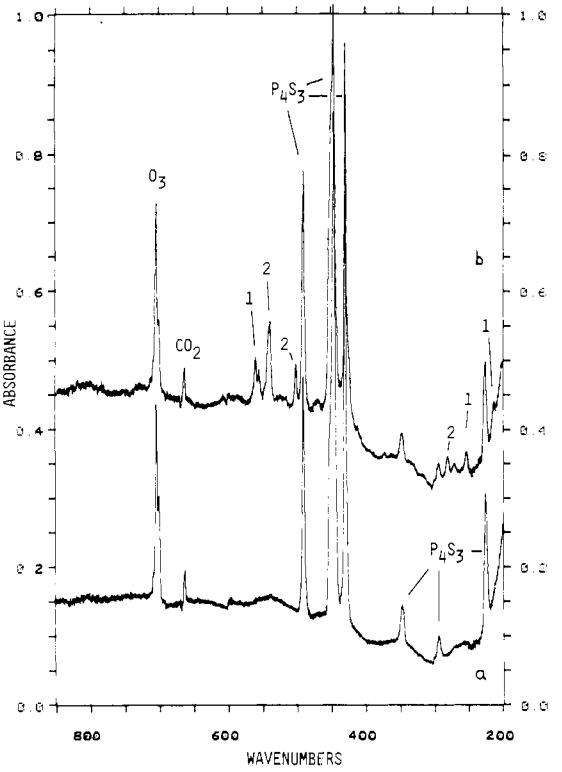

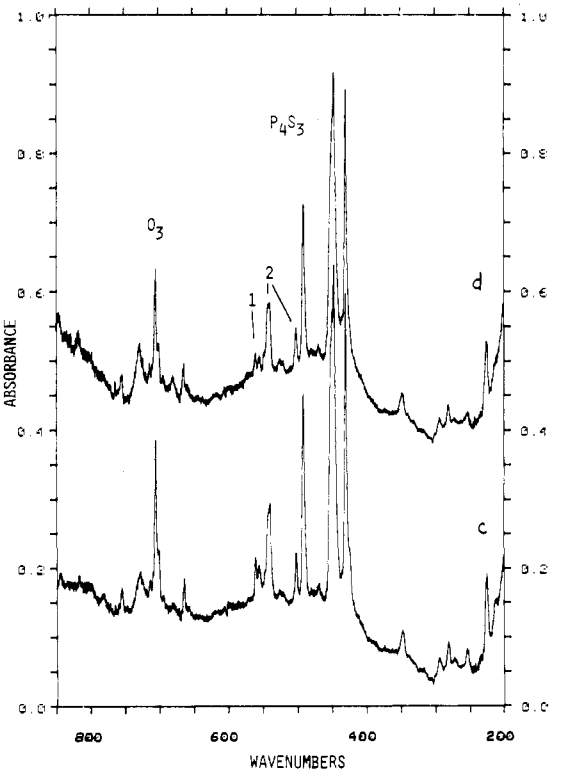

Figure 3. The 200–850-cm^{-1} region of the spectra presented in Figure 2.

increased these bands and weak satellite features in the terminal PO stretching region at 1281.5, 1262, and 1239 cm^{-1} by another 40% and slightly decreased the P_4S_3 precursor absorptions; the latter spectrum is illustrated in Figures 2b and 3b for the upper and lower regions. Full arc photolysis ($\lambda > 220$ nm) for 30 min (Figures 2c and 3c) increased bands 1 and 2 but increased group 2 more (35%) than group 1 (15%). Ultraviolet photolysis also increased the weak 1281.5-cm^{-1} satellite feature and produced a number of weaker bands at 845, 817, 753, 727, and 523 cm^{-1}. Full arc photolysis for an additional 60 min decreased group 1 more (25%) than group 2 (5%) band intensities, increased the latter bands, and further decreased the P_4S_3 absorptions. Final

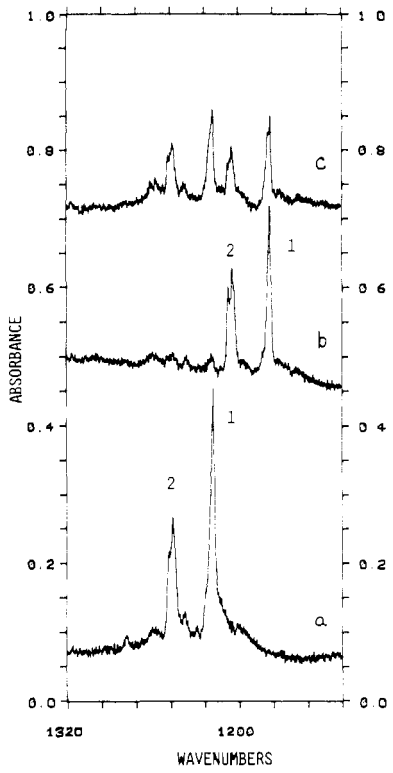

Figure 4. Terminal P–O stretching region in the spectra of matrices obtained by codeposition of P_4S_3: (a) with $Ar/O_3 = 75/1$ after 30 min of 590–1000-nm photolysis; (b) with $Ar/^{18}O_3 = 150/1$ 98% ^{18}O enriched, after 65 min of 590–1000-nm photolysis; (c) with $Ar/^{16,18}O_3 = 150/1$, 50% ^{18}O enriched, after 40 min of 590–1000-nm photolysis.

full arc photolysis for 120 min more continued this trend, as is shown in Figures 2d and 3d, clearly demonstrating that bands 1 and 2 belong to different species and that secondary photolysis leads to a small yield of other absorptions that are given in Table I.

Five experiments were done with $^{16}O_3$ and P_4S_3 using different reagent concentrations, photolysis wavelengths, and photolysis periods. The behavior outlined in Figures 2 and 3 was reproduced in all experiments. Following red-light photolysis ($\lambda > 590$ nm) in other experiments, exposure to visible ($\lambda > 420$ nm) radiation further decreased the C bands and increased bands 1 and 2 (depending on the period of previous 590-nm photolysis) and produced the 727-cm^{-1} band. After photolysis, several samples were annealed to 30–35 K and no significant changes were observed.

Infrared spectra from a P_4S_3 and $^{18}O_3$ sample revealed shifted absorptions that are given in Table I. The ozone satellite bands were appropriately displaced to 975.2 and 660.4 cm^{-1}. Red-light photolysis produced strong group 1 and 2 bands in the 1200-cm^{-1} region, which exhibited large oxygen-18 shifts to 1203.9 and 1176.3 cm^{-1} as shown in Figure 4b; the weak oxygen-16 counterparts were detected at 1281.4 and 1247.4 cm^{-1} as well. Lower frequency bands 1 and 2 exhibited smaller shifts ranging from 0.0 to 1.6 cm^{-1}. Full arc photolysis for 45 min increased both band groups, but group 2 increased more (65%) than group 1 (50%). An additional 60-min photolysis decreased group 1, increased group 2, and produced weak bands at 1237.5, 723.6, and 697.8 cm^{-1}. A final 80-min full arc photolysis continued this trend, decreasing group 1 (20%), and increasing group 2 (10%) and the latter weak bands. Another experiment was performed with a mixed isotopic ozone sample. Red-light photolysis produced the sharp group 1 and 2 bands near 1200 cm^{-1} with their pure isotopic values and no evidence of splitting (Figure 4c) and produced unresolved intermediate bands in the lower frequency region.

Calculations

The SCF structures calculated for three P_4S_3O isomers are compared with the P_4S_3 geometry in Figure 5. The calculated

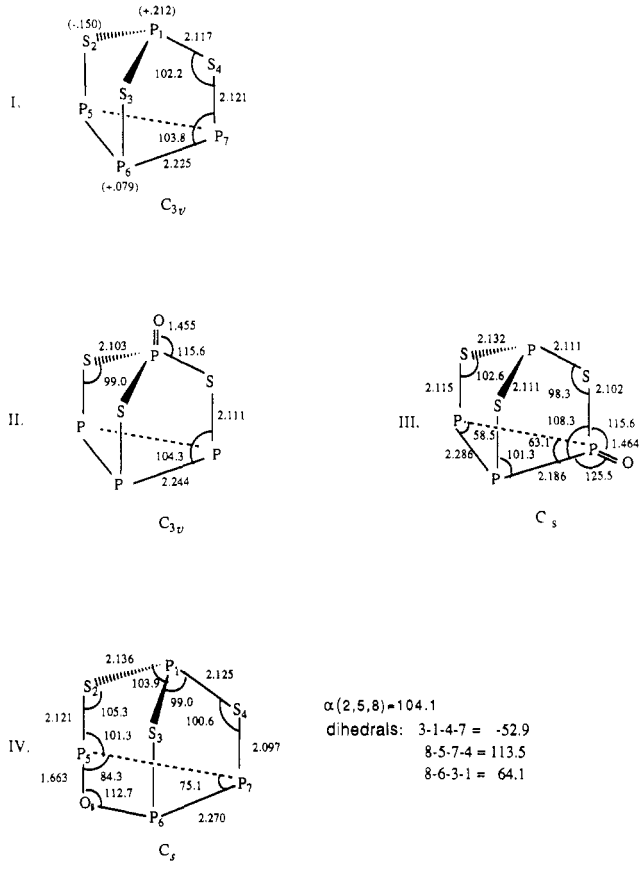

Figure 5. SCF structures calculated for P_4S_3 and three P_4S_3O isomers.

Table II. Energies (hartrees), Relative Energies (kcal/mol), and Zero Point Energies (kcal/mol) for Three P_4S_3O Isomers

isomer	E	ΔE	ZPE	ΔH_0[a]
II	−71.95072	0.0	11.9	0.0
III	−71.93642	+9.0	11.8	+8.9
IV	−71.95245	−1.1	11.7	−1.3

[a] $\Delta H_0 = \Delta E + \Delta(ZPE)$.

structure for P_4S_3 is in excellent agreement with the experimental structure;[2] bond lengths are within ±0.01 Å and angles are within ±1°. Mulliken populations are displayed for the latter compound as well. The total and relative energies for the three P_4S_3O isomers are listed in Table II.

Discussion

The new photochemical product species will be identified and compared to the analogous P_4 reaction products.

Primary Products. The satellite features at 1101.5, 1033.2, and 700.1 cm^{-1} on the ozone absorptions at 1104.2, 1039.5, and 703.8 cm^{-1} are assigned to the P_4S_3--O_3 complex, which photolyzes with red light to give the photochemical products observed here. This red-light photolysis of O_3 has been observed in complexes with PH_3, P_4, and PCl_3.[11-13,18,20] In the red excited state (Chappuis band) for ozone in the complex, ozone is activated for transfer of an O atom to P_4S_3 forming a terminal PO bond and giving P_4S_3O and O_2 as major reaction products.

The P_4S_3--O_3 complex is comparable in strength to the P_4--O_3 complex[11] but is stronger than the H_3P--O_3 complex[18] based on the shifted ozone complex bands. In the P_4 case, the perturbed ν_1^c and ν_2^c modes are the same within experimental error[11] and the ν_3^c mode has been observed[12] at 1033.5 cm^{-1}, a slightly smaller shift than found for ν_3^c of the P_4S_3--O_3 complex.

(18) Withnall, R.; Hawkins, M.; Andrews, L. *J. Phys. Chem.* **1986**, *90*, 575.
(19) Withnall, R.; Andrews, L. *J. Phys. Chem.* **1987**, *91*, 784.
(20) Moores, B. W.; Andrews, L. *J. Phys. Chem.* **1989**, *93*, 1902.

The strong, sharp red photolysis product bands at 1247.4 and 1218.4 cm^{-1} are in the terminal PO stretching region near those for P_4O (1240.5 cm^{-1}),[11,12] H_3PO (1240.2 cm^{-1}),[19] and PO itself (1218.3 cm^{-1})[21] and are characterized by $^{16}O/^{18}O$ ratios (1218.4/1176.3 = 1.0358; 1247.4/1203.9 = 1.0361) that are near the value for diatomic PO (1218.3/1173.6 = 1.0385).[17] The weak 1262 and 1239-cm^{-1} satellite bands and the sharp splitting at 1250.8 cm^{-1} are associated with the strong group 2 band at 1247.4 cm^{-1}. In fact the stability of the 1218.4-cm^{-1} band on annealing and its ^{18}O counterpart at 1176.3 cm^{-1} (as compared to $P^{18}O$ at 1173.1 cm^{-1}) differentiate the carrier of this absorption from the PO diatomic molecule.[21]

Of more importance the terminal PO product absorptions accompany other bands associated by photolysis behavior as groups 1 and 2. While there is no obvious P_4S_3 or O_3 concentration dependence for the relative intensities of group 1 and 2 bands produced by 590-nm photolysis, the group 1 bands are clearly decreased more efficiently by full arc photolysis, and this difference provides a basis for the observation and characterization of two distinctly different product species. These products are now identified as structural isomers of P_4S_3O formed by terminal O atom attachment to the P_4S_3 precursor molecule.

The above evidence shows that bands 1 and 2 are due to terminal-oxide adducts of P_4S_3. Two structural possibilities exist: apex attachment of oxygen retains the C_{3v} symmetry of P_4S_3, and base attachment lowers the symmetry to C_s. It is not immediately obvious, however, which group of bands belongs to which structure. Both isomers contain new bands near 550 cm^{-1} due to the product counterparts of the strongest P_4S_3 infrared absorption at 446 cm^{-1}. This polarized band in the Raman spectrum is due to a symmetric stretching mode (ν_2) involving the P–S–P bridge bonds. It is expected that this mode couples more with the terminal PO stretch in the C_{3v} species. The 558.8-cm^{-1} band exhibited a 1.6 cm^{-1} ^{18}O shift whereas the 538.3-cm^{-1} band showed only a 0.5-cm^{-1} shift, which suggests that the former is due to the C_{3v} and the latter the C_s species. Furthermore, a larger displacement from the 446-cm^{-1} P_4S_3 mode is expected for the C_{3v} species with the greater opportunity for interaction with sulfur, which also indicates assignment of the higher 558.8-cm^{-1} band to the C_{3v} species. The sharp 500.2-cm^{-1} band is most probably a product counterpart of the sharp 489.5-cm^{-1} P_4S_3 band, which was observed only for the isomer of lower symmetry. The product bands in the 200-cm^{-1} region show ^{18}O shifts and probably involve mixed cage and oxygen substituent deformation modes. In the C_{3v} species the doubly degenerate oxygen deformation and cage modes will mix and the ^{18}O shift will be shared between modes as found in the two low-frequency group 1 modes with small ^{18}O shifts, in contrast to the single 279.3-cm^{-1} group 2 band, which exhibited a large ^{18}O shift owing to the lack of mode mixing. We conclude that the group 1 bands are most likely due to the C_{3v} apex terminal oxygen-bonded P_4S_3O species (II) and that the group 2 bands are due to the C_s base oxygen-bonded isomer (III).

Comparisons. It is interesting to compare the terminal PO modes of II and III with each other and with those of P_4O (1240 cm^{-1}) and P_4O_7 (1379 cm^{-1}).[22] Since the terminal PO motions are far removed from motions of the cage, they can be used to represent bonding effects in the molecules. The terminal PO bond has been examined theoretically.[23,24] The best rationale involves a strong σ bond (3p–2p) augmented by some degree of back-bonding to p and d orbitals on phosphorus, which in effect gives some "double-bond" character often used to describe the terminal PO bond. Accordingly, electronegative substituents bonded to P increase the positive charge at phosphorus, the back-bonding, and the PO fundamental frequency. This effect is found in the two series H_3PO, Cl_3PO, and F_3PO and $(CH_3)_3PO$, $(CH_3S)_3PO$, and $(CH_3O)_3PO$.[25,26] On the other hand, the influence of an S–P bond on the terminal PO fundamental has been rationalized as a drift of π-electron density from the PO bond into vacant d orbitals on sulfur.[27] The latter effect must dominate in C_{3v} P_4S_3O as the PO fundamental (1218 cm^{-1}) is lower than that in P_4O (1240 cm^{-1}). Similar oxygen substitution in the cage increases the PO fundamental although the only compound available for comparison is P_4O_7 (1379 cm^{-1}), which has six bridge-bonded oxygen atoms.[22] In contrast, the PO fundamental in the C_s isomer P_4S_3O (1247 cm^{-1}) is slightly higher than that in P_4O (1240 cm^{-1}). Here the S–P–O angle is probably larger and overlap between S and P orbitals less effective, and the electronegative substituent effect dominates. The effect of a single sulfur bearing substituent is larger in $(CH_3)_2(CH_3S)PO$ (1182 cm^{-1}) as compared to $(CH_3)_3PO$ (1160 cm^{-1}) than in P_4S_3O (C_s structure) as compared to P_4O.

Finally, which terminal isomer is more stable? The larger yield of the C_{3v} species in spite of one-third as many sites for attachment argues that the C_{3v} isomer (II) is more stable than the basal isomer (III). The known structures of P_4S_5 and P_4S_7 provide some information in this regard.[10] In the latter the two terminal S atoms are attached to P atoms with three bridging sulfur atoms and not P atoms with only two bridging sulfur atoms, but in the former the terminal S atom is attached to the P with two bridging sulfur atoms and not the P atoms with one or three bridging sulfur atoms. Full arc photolysis does decrease the C_{3v} isomer more efficiently, which may be due to greater reactivity in the excited state.

The electron densities obtained from the Mulliken population analysis for P_4S_3 are in qualitative agreement with the observations discussed above: The unique (apex) phosphorus is the most likely site for attack by an electronegative oxygen. The structure of the parent P_4S_3 is only slightly modified by substitution of an oxygen atom in the apex position. Since O atom substitution at one of the basal positions causes a significant reduction in symmetry, this results in a more distorted structure, with P–P bonds that differ from each other by ~0.1 Å and that bracket the P–P bond length of P_4S_3.

As inferred from the experimental observations, the C_{3v} structure is predicted by theory to be lower in energy that the C_s structure. At the MP2 level of theory and including corrections for vibrational zero point energy (ZPE), the predicted energy difference is 8.9 kcal/mol. On the other hand, the predicted frequencies are in the reverse order from the experimental ones. After scaling, since SCF calculations commonly predict vibrational frequencies that are too large,[28] the predicted frequencies for the C_{3v} and C_s P_4S_3O structures are 1205 and 1182 cm^{-1}, respectively. This small difference, however, is probably inside the error bounds of the calculations.

Secondary Products. There was a variable yield of the weaker satellite bands in the 1200- and 700-cm^{-1} regions produced by full arc photolysis in the experiments performed. Two different processes can contribute to these absorptions, the decomposition of P_4S_3O and the reaction of $O(^1D)$ produced on full arc photolysis with P_4S_3 and/or P_4S_3O. The 1281.5, 753-, 727-, and 523-cm^{-1} bands increased markedly on full arc photolysis. In P_4/O_3 systems, the major reaction on full arc photolysis was the formation of oxo-bridged P–O–P bonds.[11,12] The 753- and 728-cm^{-1} bands fall below the antisymmetric stretching mode of oxo-bridged tetrahedral P_4O at 856 cm^{-1}, but they exhibit almost the same $^{16}O/^{18}O$ ratio (1.042 ± 0.001), which characterizes the 753- and 727-cm^{-1} bands as antisymmetric P–O–P vibrations. Since unreacted P_4S_3 exceeds P_4S_3O by a factor of approximately 4, based on 446-cm^{-1} P_4S_3 absorbance relative to 558- plus 538-cm^{-1} P_4S_3O absorbance in Figure 3b, the major full arc photolysis product absorption at 727 cm^{-1} is tentatively assigned to oxo-bridged P_4S_3O (IV). The weaker 523-cm^{-1} band shows the same photolysis behavior and

(21) Withnall, R.; Andrews, L. *J. Phys. Chem.* **1988**, *92*, 4610.
(22) Mielke, Z.; Andrews, L. *J. Phys. Chem.* **1989**, *93*, 2971.
(23) Schmidt, M. W.; Gordon, M. S. *J. Am. Chem. Soc.* **1985**, *107*, 1922.
(24) Streitwieser, Jr., A.; McDowell, R. S.; Glaser, R. *J. Comput. Chem.* **1989**, *8*, 788.
(25) Goubeau, J.; Lentz, A. *Spectrochim. Acta* **1971**, *27A*, 1703.
(26) Pantzer, R.; Schmidt, W.; Goubeau, J. *Z. Anorg. Allg. Chem.* **1973**, *395*, 262.
(27) Blindheim, U.; Gramstad, T. *Spectrochim. Acta* **1965**, *21*, 1073; **1969**, *25A*, 1105.
(28) Pople, J. A.; Schlegel, H. B.; Raghavachari, K.; DeFrees, D. J.; Binkley, J. S.; Frisch, M. J.; Whiteside, R. A.; Hout, R. J.; Hehre, W. J. *Int. J. Quantum Chem. Symp.* **1981**, *S15*, 269–278.

is assigned to the strongest P–S stretching mode for this species, analogous to the 446-cm^{-1} band for P_4S_3.

The 753-cm^{-1} band appears to track with the sharp 1281.5-cm^{-1} band in the terminal PO stretching region throughout the photolyses performed in these experiments. The 1281.5-cm^{-1} band exhibits an appropriate isotopic ratio (1281.5/1237.5 = 1.0356) for a P–O stretching fundamental. The 1281.5- and 753-cm^{-1} absorptions are tentatively assigned to a $P_4S_3O_2$ species with one terminal and one bridged oxygen. Of the three possible structural isomers, the most likely one involves a common phosphorus atom. In this case, the effect of the bridging oxygen on the terminal PO fundamental is maximized (i.e. blue-shifted from 1247 to 1281 cm^{-1}). It should be noted that adding six bridging oxygen atoms to terminal P_4O shifts the PO fundamental from 1240 to 1379 cm^{-1}, an average of 23 cm^{-1} per bridging oxygen.

The structure of the oxo-bridged P_4S_3O isomer (IV) is shown in Figure 5. As one would expect, the PO bond lengths in this isomer are 0.2 Å longer than those in the isomers with terminal PO bonds. The vibrational frequencies associated with the P–O–P bridge (688 and 736 cm^{-1} after scaling) are accordingly smaller than those in the other two isomers. One of these apparently corresponds to the 727-cm^{-1} band observed for this isomer.

It is not surprising that the isomer containing the P–O–P bridge is predicted to be lower in energy than both of the other two isomers. Similar results have been obtained from ab initio calculations on the analogous P_4O isomers[29,30] and the H_3PO and H_2POH isomers.[31] At the SCF level of theory, the energy difference between the C_{3v} and bridged isomers is >10 kcal/mol. However, addition of correlation corrections via second-order perturbation theory reduces this to just 1.1 kcal/mol. It is possible that the use of larger basis sets and more extensive correlation corrections might reverse the energy order of these two isomers.

The experimental observations show that the terminal isomers are formed by red-light photolysis of the precursor ozone complexes and that the oxo-bridged isomers are formed by UV irradiation, which gives $O(^1D)$ for insertion into a P–P bond.[11,12,18,19] Although the terminal phosphoryl isomers are less stable energetically than the oxo-bridged isomers, a large barrier separates the two isomers (70 kcal/mol in the case of H_3PO and H_2POH).[31] Even though the attachment of terminal oxygen to phosphorus is highly exothermic (130–140 kcal/mol),[32] the cold matrix relaxes this internal energy before arrangement to the more stable oxo-bridged isomer can take place.

The small decrease in group 1 and 2 absorptions on full arc photolysis is ascribed to the secondary reaction suggested above and/or decomposition, but no decomposition product can be clearly indentified. The weak 845- and 817-cm^{-1} bands observed after prolonged full arc photolysis fall above the terminal PS stretching region (750-720 cm^{-1})[4,33] but in the P–O–P stretching region. Unfortunately, the yield was insufficient in the ^{18}O experiment to give counterparts. The weak 845- and 817-cm^{-1} bands are appropriate for $P_xS_yO_z$ fragments that cannot be identified from the present data.

Conclusions

The codeposition of P_4S_3 and O_3 (and $^{18}O_3$) with excess argon at 12 K resulted in a P_4S_3--O_3 complex characterized by perturbed ozone infrared absorptions. Red-light photolysis decreased the complex bands and produced two groups of intense new product absorptions; ultraviolet irradiation decreased the two groups in different proportions and increased four other absorptions. In similar P_4 experiments, red-light photolysis produced primarily terminal P_4O, and ultraviolet irradiation gave oxo-bridged tetrahedral P_4O; analogous behavior has been found for P_4S_3.

Each group of absorptions produced by red photolysis included terminal PO and symmetric P–S–P stretching modes, which characterized the two isomers of P_4S_3O with terminal oxygen at the apex and base phosphorus positions of the bird cage P_4S_3 structure. The larger yield of the C_{3v} species (II) in spite of one-third as many sites for attachment for terminal oxygen as the C_s species (III) argues that the former is more stable; this point is substantiated by electronic structure calculations. The other absorptions favored by ultraviolet photolysis include antisymmetric P–O–P and symmetric P–S–P stretching modes, which tentatively identify the oxo-bridged P_4S_3O isomer, and different terminal PO and antisymmetric P–O–P stretching modes, which suggest a secondary $P_4S_3O_2$ product.

Acknowledgment. We appreciate financial support from NSF Grants CHE 88-20764 and CHE 89-11911 and AFOSR Grant 90-0052.

(29) McCluskey, M.; Andrews, L. To be published.
(30) Lohr, L. L. *J. Phys. Chem.* **1990**, *94*, 4832.
(31) Schmidt, M. W.; Yabushita, S.; Gordon, M. S. *J. Phys. Chem.* **1984**, *88*, 382.
(32) Mellor, J. W. *Inorganic and Theoretical Chemistry*; Wiley-Interscience: New York, 1971; Vol. VIII, Suppl. III, Phosphorus.
(33) Mielke, Z.; Brabson, G. D.; Andrews, L. To be published.